Polymer Testing 30 (2011) 861–866

Contents lists available at SciVerse ScienceDirect

Polymer Testing

journal homepage: www.elsevier.com/locate/polytest

Test method

Observation of damage evolution in polymer bonded explosives using acoustic emission and digital image correlation

Xian Wang [a,b], Shaopeng Ma [b,*], Yingtao Zhao [b], Zhongbin Zhou [a], Pengwan Chen [a]

[a] State Key Laboratory of Explosion Science and Technique, Beijing Institute of Technology, Beijing 100081, China
[b] School of Aerospace Engineering, Beijing Institute of Technology, Beijing 100081, China

ARTICLE INFO

Article history:
Received 8 June 2011
Accepted 13 August 2011

Keywords:
Polymer bonded explosives
Acoustic emission
Digital image correlation
Damage localization

ABSTRACT

The Acoustic Emission (AE) and Digital Image Correlation (DIC) methods have been combined to measure and evaluate the damage evolution of Polymer Bonded Explosives (PBXs) under uniaxial compression. The global damage evolution was measured by AE and the local (spatial) distribution of damage observed by DIC. It was found that a Dominant Localization Band (DLB) plays a key role in the damage and fracture of the specimen. Because of the existence of the DLB, the specimen is essentially a structure with a weak plane during the nonlinear stage and, therefore, the nonlinear behavior is the average response of the structure. A simple model has been proposed to describe the mechanical behavior of the specimen based on the DLB and the measured damage parameters. The non-linear stress–strain relationship of the specimen is then deduced from the model and verified by experiment.

1. Introduction

Polymer Bonded Explosives (PBXs) are one of the most important solid energetic materials used in a variety of weapons. PBXs are brittle and heterogeneous materials, in which the highly brittle crystalline explosives (90–95% in weight) are distributed in a soft polymer binder [1,2]. During filling, storage and transportation of weapons, PBXs in warheads are subject to various loads and are prone to damage from micro-cracks initiated from widely distributed manufacturing defects within the material. Damage in PBXs not only degrades its mechanical properties, but also greatly affects its combustion and detonation ability. Therefore, the inspection of damage evolution in PBXs subject to load is of great importance for characterizing of the material as well as for the design of new PBXs [3].

In published works [4,5], direct observation techniques, such as Scanning Electron Microscopy (SEM) [4] and Computed Tomography (CT) [5], have been used to evaluate the damage of PBXs. These methods can obtain the spatial distribution of damage in a slice or for the whole specimen, but they are often unable to view this during loading and, hence, are not able to obtain data about damage evolution. Another widely used damage measurement technique, Acoustic Emission (AE) [6], has also been used to evaluate the damage of PBXs by collecting and analyzing the wave signal emitted by micro-cracks during deformation and failure of the specimen. Compared with SEM and CT, the data acquisition in AE experiments is continuous and real-time, thus damage evolution can be measured during the loading process. However, when using AE, the spatial distribution of damage is difficult to identify. Generally, the damage given by AE data is often evaluated by a statistical measurement of energy or a number of AE events collected from one or two sensors. Although the damage position can be determined using AE positioning techniques, this kind of experiment is often very difficult to realize in small specimen experiments.

The occurrence of damage, especially the damage concentration in a specimen, will inevitably reveal itself in the deformation field of the specimen surface. Therefore,

* Corresponding author. Tel.: +86 10 68912736.
E-mail address: masp@bit.edu.cn (S. Ma).

0142-9418/$ – see front matter © 2011 Elsevier Ltd. All rights reserved.
doi:10.1016/j.polymertesting.2011.08.006

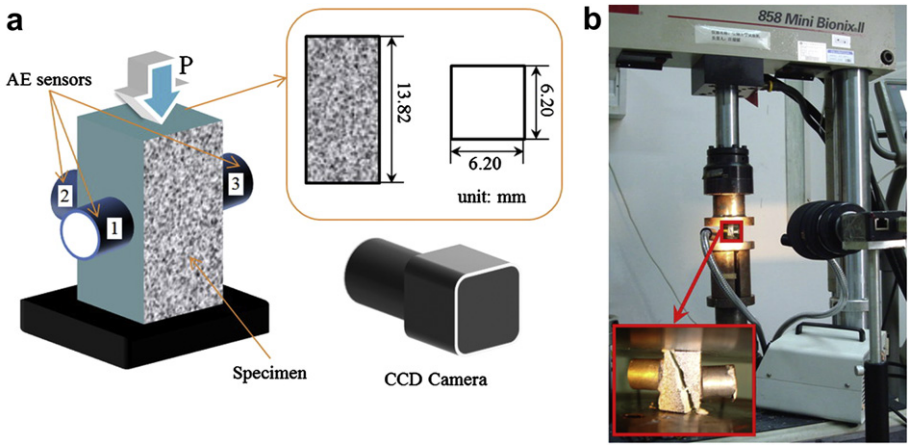

Fig. 1. Schematic of experiment; (a) experimental system and specimen size; (b) experimental scene.

whole field photomechanics methods, for example Digital Image Correlation (DIC) [7], have also been used to reveal damage distribution. Using a continuous image capturing system, DIC can measure deformation fields of a specimen surface in real time, such that it can be used to analyze the spatial distribution of damage on the specimen's surface for different load levels. If AE and DIC can be combined to measure the damage of material under loading then global characteristics for damage evolution can be obtained and the spatial distribution of the damage can be analyzed [8,9].

In this paper, uniaxial compression experiments of inert simulated PBXs have been performed. The damage evolution of the specimens was measured and evaluated using AE and DIC and the spatial evolution characteristics of damage are identified based on DIC results. Based on these results, a very simple damage localization based model has been proposed to explain the nonlinear mechanical behavior of uniaxially compressed PBXs.

2. Experiment and results

2.1. Experimental setup

A typical uniaxial compression experiment was carried out on a specimen made of inert simulated PBX as follows. A square column-shaped specimen of size $13.82 \times 6.20 \times 6.20$ mm^3 was compressed in a MTS-858 (Mini Bionix) test machine and loading was increased in displacement control mode with a speed of 0.03 mm/min. As shown in Fig. 1, one side of the specimen surface was painted with a speckle pattern and images of it captured by a Basler A641f digital CCD camera. The resolution of the camera was 1624×1236 pixels and the image acquisition rate was 15 fps (frame per second). Three AE sensors were positioned on the other three surfaces of the specimen to monitor micro-cracking.

2.2. Damage evolution measured by AE

The result of a typical experiment is described as follows, with the nominal stress-strain curve of the specimen given in Fig. 2. For AE measurement, an elastic wave that is released by the sudden appearance of a micro-crack is generally called an AE event and can be expressed by a voltage variation of an AE sensor as shown in the left-top of Fig. 2. AE events collected by sensor 2 are also plotted on the figure with each event expressed as a vertical short line, the height of which represents the energy of the event calculated by the integration of the square wave signal.

The normalized accumulated energy of AE events was used to evaluate the damage. Considering all three AE sensors, a damage variable D can then be defined as in Eq. (1),

$$D_\varepsilon = \frac{1}{3}\sum_{i=1}^{3}\left(\int_0^{\varepsilon} P_{i\varepsilon}\,d\varepsilon \Big/ \int_0^{\varepsilon_c} P_{i\varepsilon}\,d\varepsilon\right), \tag{1}$$

where ε is the nominal strain of the specimen, ε_c is the failure strain, and $P_{i\varepsilon}$ is the energy of the ith sensor at the loading level of ε.

In Fig. 2, the variation of damage D relative to the stress-strain curve of the specimen is plotted. From this curve, the global evolution of damage can be identified. Here, it can be seen that damage increases slowly and steadily at the beginning of the loading procedure and then increases rapidly towards the end. For a specimen of this size, only three AE sensors could be positioned on the surface and locating an AE event is difficult. Therefore, the spatial distribution of the damage and its evolution cannot be observed by AE.

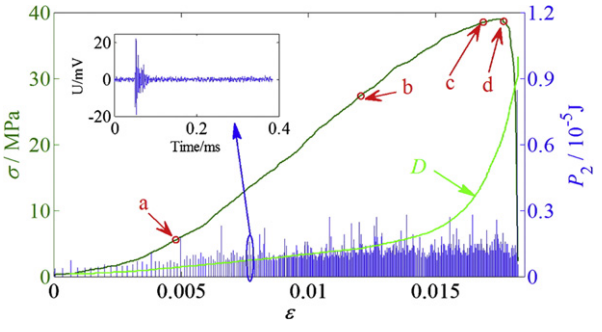

Fig. 2. σ-ε, P_2-ε and D-ε curve of the specimen.

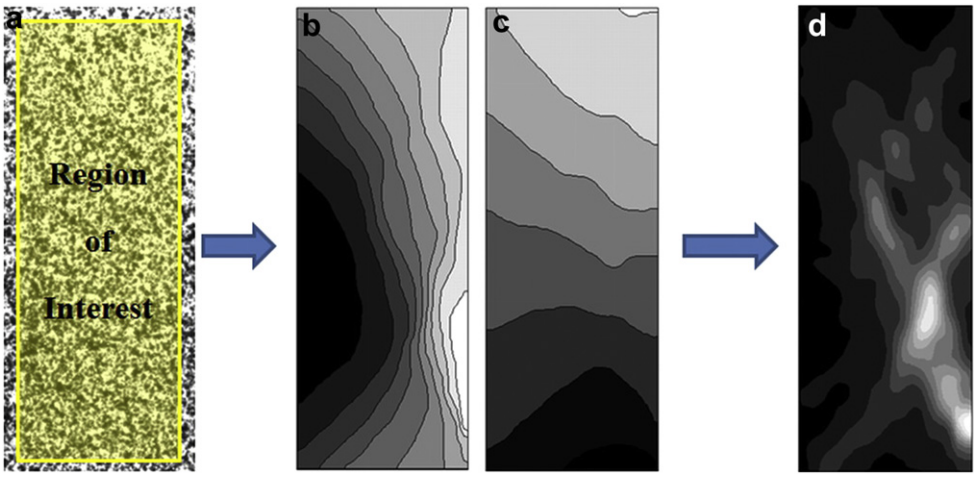

Fig. 3. Calculation process of DIC; (a) digital speckle image; (b) horizontal displacement field; (c) vertical displacement field; (d) maximum shear strain field.

2.3. Damage distribution evaluated by DIC

DIC is widely used for displacement and strain field measurement due to its characteristics of non-contact, high precision and simple measuring requirements. Data analysis of DIC is shown in Fig. 3. By matching a sequence of digital speckle images (as shown in Fig. 3a) captured at different loading levels in an experiment, the displacement fields of the whole loading procedure can be obtained (Fig. 3b and c). Furthermore, the stain field can be deduced by numerical differentiation of the displacement fields (Fig. 3d).

The maximum shear strain fields of the specimen surface at four typical loading levels, marked with circles in Fig. 2, are shown in Fig. 4.

It can be seen that the strain fields are homogeneous at the beginning, but become heterogeneous at a later loading stage. Further comparison between the damage evolution curve in Fig. 2 and the strain field evolution from the DIC results shows that the homogeneous strain fields occur at the slow and steady increasing stage of damage. The appearance of the strain localization occurs when the damage begins to speed up with the appearance of the macro-crack fractures in the specimen when the damage reaches its maximum value. Considering the specimen is complete and homogeneous at the beginning, the heterogeneous distribution of the deformation field must be caused by the localized damage. That is to say that the strain localization band corresponds to the damage localization band. Based on this, the strain field evolution from the DIC experiment can be used to analyze the damage distribution. It can be seen that the damage is homogeneous at the early loading stage. When the specimen is loaded close to the peak of the stress-strain curve, an obvious damage localization band appears. This band is then "refined" and "brightened" gradually as the loading continues. Finally, a macro-crack appears within the band and totally fractures the specimen.

Furthermore, it can be seen that several localization bands appear at the late loading stage, but one of them (marked with the dotted line in Fig. 5a) is much larger and

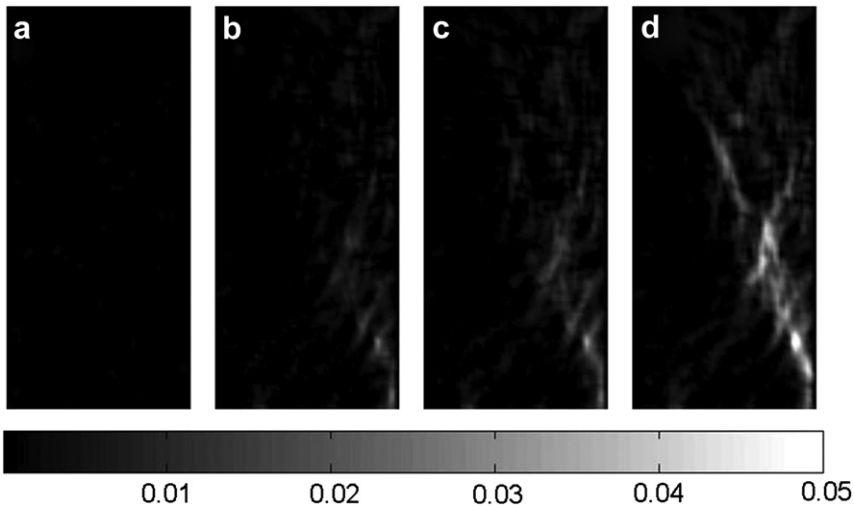

Fig. 4. Maximum shear strain fields at four typical loading levels (the four levels are marked a to d in Fig. 2).

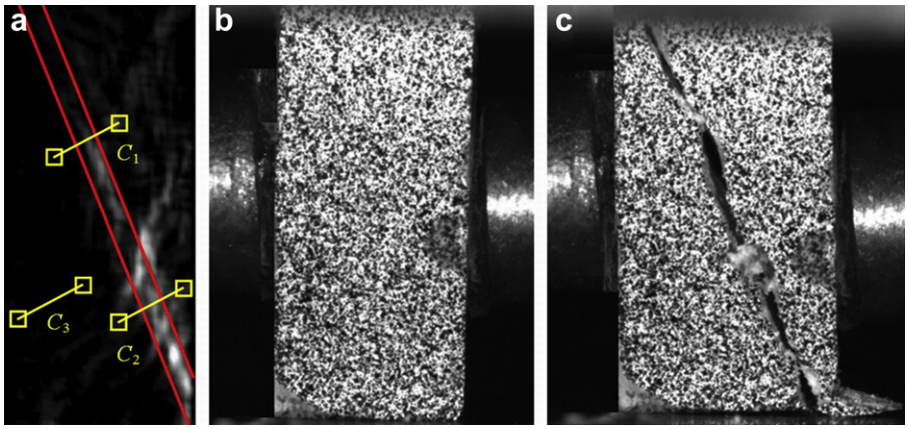

Fig. 5. Dominant localization band; (a) the band; (b) the specimen fractured along the DLB. The random dots on the specimen surface are the painted speckle used in the experiment.

more active. Fig. 5b shows that the specimen is finally fractured along this localization band (the band is termed the Dominant Localization Band in this paper, abbreviated as DLB).

When the DLB appears, the specimen essentially becomes a structure with a weak plane. This can be verified by the comparison of the movement of different "virtual extensometers" in Fig. 5a. Using the displacement field from DIC, the relative dislocation of the 2 points could be evaluated. Fig. 6 shows that the dislocation of C_3, which is located outside of DLB, is much smaller and almost consistent with the theoretical dislocation (C_{th} in the figure) evaluated from the linear elastic model. The dislocation of C_1 and C_2, located across the DLB, is similar to that of C_3 before the DLB appears (stage I), but is quite different when the DLB is present (stage II). It is shown that the dislocation of C_1 and C_2 is much larger than that of C_3 after the appearance of DLB. This indicates that the material within the DLB is damaged and, therefore, is weaker than that outside of the DLB. With increasing load, the difference becomes much larger and this indicates that the material within the DLB becomes much weaker. Furthermore, the consistency between C_1 and C_{th} indicates that the material outside of the DLB stays linear elastic during the whole loading procedure. Therefore, the appearance and damage evolution of the DLB could be concluded to be the key to damage localization and the nonlinear behavior of the specimen.

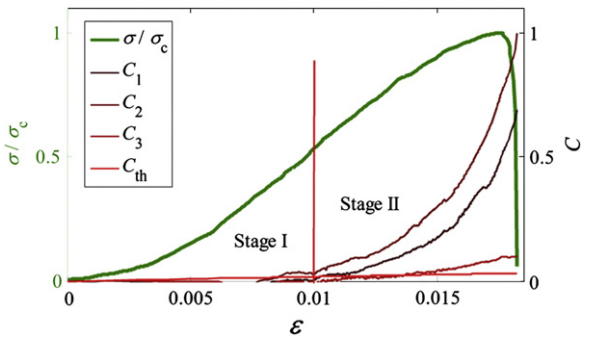

Fig. 6. Dislocation of different "extensometers" (C_1, C_2, C_3 are marked in Fig. 5a, C_{th} represents the theoretical dislocation of C_3 that has been calculated from the elastic displacement field).

3. A model to explain the nonlinear behavior of PBXs

In existing literature, a number of complicated mechanical models, for example the strain gradient models [10,11], have been introduced to explain the nonlinear behavior of a specimen made from such brittle materials. Damage models [12] in which the elastic modulus of the material decreases with increasing load have also been used to explain such behavior. Compared with the strain gradient models, this damage model is much simpler and more appropriate for practical use. Here, the damage variable is taken to express the degree of degradation of the materials and, as shown in the previous figures, the stress-strain curve of PBXs includes a linear part at the earlier loading stage and a nonlinear part later on. This section aims to construct a model to explain the nonlinear part of the specimen.

3.1. Model

As previously mentioned, the damage mechanism of PBXs is mainly due to the appearance and evolution of DLB. Before DLB appearance, the specimen is homogenous, the damage of the specimen is low and the stress-strain curve is linear. After the appearance of DLB, the damage in the specimen increases, the specimen becomes a structure and the stress-strain curve becomes nonlinear. Therefore, the specimen can be divided into 2 different parts, as shown in Fig. 7, the damaged part (DLB) and the undamaged part (UDP). UDP is characterized by the elastic modulus E, which stays constant during the whole loading procedure. DLB is characterized by the secant elastic modulus E', which varies according to Eq.(2),

$$E' = (1 - D)E, \tag{2}$$

where D is the damage of the material as measured by the AE method. When there is no damage, $D = 0$, $E' = E$, and

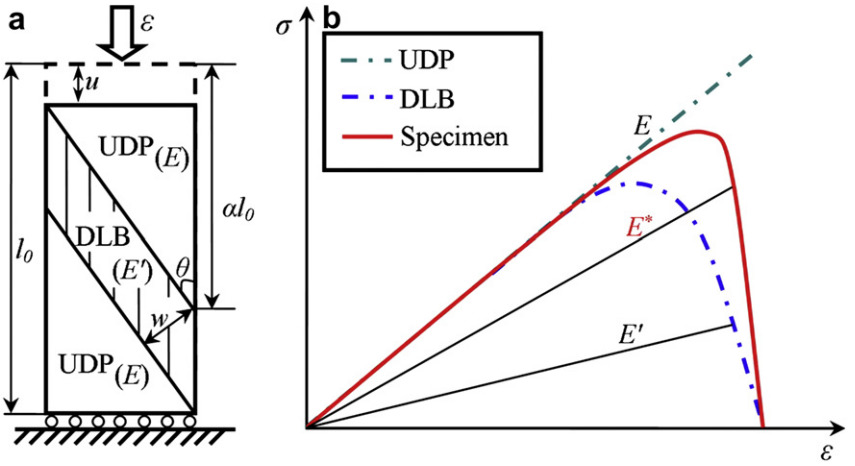

Fig. 7. The schematic of the model; (a) the division of the specimen; (b) the elastic modulus of different parts.

the specimen is complete without any structure. When $D \neq 0$, $E' < E$, and the specimen is a structure with a weak plane.

Let ε represents the nominal strain of the specimen along the loading direction such that,

$$\varepsilon = u/l_0, \tag{3}$$

where u is the reducing length of the specimen and l_0 is the initial length of the specimen. The relationship between the nominal strain and the stress on the loading end of the specimen can be deduced as,

$$\frac{\sigma}{E}\alpha l_0 + \frac{\sigma}{E'}(1-\alpha)l_0 = \varepsilon l_0, \tag{4}$$

where

$$\alpha = 1 - \frac{w}{l_0 \sin\theta}, \tag{5}$$

α is the geometric parameter of the DLB that represents the percentage of UDP in the specimen along the loading direction, w is the width, and θ is the inclination angle of the DLB.

Substitute Eq. (2) into Eq. (4) and the final relationship between the nominal stress and strain of the specimen could be obtained as,

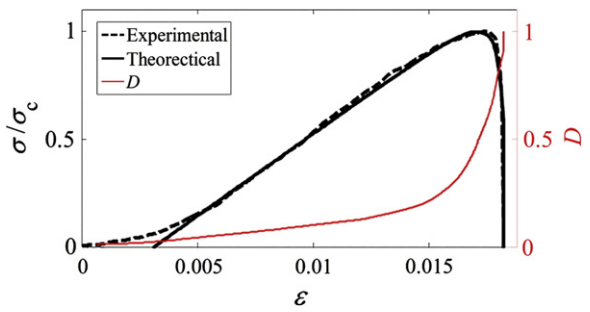

Fig. 8. Comparison of the stress-strain curve from theoretical and experimental results.

$$\sigma = \frac{1-D}{1-\alpha D}E\varepsilon = E^*\varepsilon, \tag{6}$$

where E^* is the equivalent secant modulus of the specimen.

Eq. (6) offers an experimental damage based model to express the uniaxial stress-strain behavior of the PBXs. It can be concluded from the equation that, when there is no damage, i.e. when $D = 0$, the equivalent modulus E^* is equal to E. When $D = 1$, then $\sigma = 0$, the specimen losses its strength and is completely fractured. When there is damage, i.e. when $D \neq 0$, then $E^* < E$ and, therefore, the stress-strain curve appears concave in the downward direction.

3.2. Verification

An experiment was performed to verify the validity of the developed model with the specimen and experimental method the same as that described in 2.2. The elastic modulus of the PBXs used in this experiment was measured to be 3.78 GPa and the parameters for the DLB were measured as $\theta = 22^\circ$ and $w = 0.52$ mm. Using this, the stress-strain curve of the specimen could be calculated and is shown in Fig. 8. It can be seen that the theoretical curve is in good agreement with the measured stress-strain curve, hence the proposed model is valid.

4. Conclusions

AE and DIC have been used to measure and evaluate the damage evolution of uniaxially compressed PBXs. The global damage evolution of a specimen was measured by the AE method and the spatial (local) evolution characteristics of the damage were analyzed using DIC measured strain fields. It has been shown that damage is the main reason for the nonlinear behavior of the specimen, and the appearance of the dominant DLB plays a key role in the behavior of the specimen. When the DLB appears, the specimen is no longer homogeneous and, therefore, the mechanical behavior of the specimen should be regarded as the average response of a structure with a weak plane.

A very simple damage localization based model has been proposed to explain the nonlinear mechanical behavior of the PBXs under uniaxial compression. The model was constructed to evaluate the response of the structure based on the measured damage parameters, the geometric parameters of DLB and the damage evolution. Experimental results have verified the validity of the proposed model and, although the proposed model is simple, it can explain the complicated nonlinear behavior of PBXs. The model is expected to be useful in the study of the mechanical behavior of other brittle materials, such as, rock, concrete, ceramic, etc.

Acknowledgments

The authors would like to thank support from the National Science Foundation of China (10972038) and the Open Foundation of State Key Laboratory of Explosion Science and Technology (BIT) (KFJJ10-8M).

References

[1] P.W. Chen, H.M. Xie, F.L. Huang, T. Huang, Y.S. Ding, Deformation and failure of polymer bonded explosives under diametric compression test, Polymer Testing 25 (3) (2006) 333–341.
[2] P.D. Peterson, K.S. Mortensen, D.J. Idar, B.W. Asay, D.J. Funk, Strain field formation in plastic bonded explosives under compressional punch loading, Journal of Materials Science 36 (2001) 1395–1400.
[3] Z.W. Liu, H.M. Xie, K.X. Li, et al., Fracture behavior of PBX simulant subject to sombined thermal and mechanical loads, Polymer Testing 28 (6) (2009) 627–635.
[4] Z.B. Zhou, P.W. Chen, F.L. Huang, S.Q. Liu, Experimental study on the micromechanical behavior of a PBX simulant using SEM and digital image correlation method, Optics and Lasers in Engineering 49 (3) (2011) 366–370.
[5] M.W. Greenaway, P.R. Laity, V. Pelikan, X-ray microtomography of sugar and HMX granular beds undergoing compaction, Shock Compression of Condensed Matter 845 (2005) 1279–1282.
[6] J.R. Luo, Y.Z. Chen, F.F. Zhao, Damage and fracture characters of PBX based on acoustic emission, Theory and Practice of Energetic Materials 5 (2003) 348–353.
[7] M.A. Sutton, Digital image correlation for shape and deformation measurements, Springer Handbook of Experimental Solid Mechanics (2008) 565–598.
[8] S.P. Ma, L.G. Wang, G.C. Jin, Damage evolution inspection of rock using digital speckle correlation method (DSCM), Key engineering materials 326 (2006) 1117–1120.
[9] X.H. Xu, S.P. Ma, M.F. Xia, F.J. Ke, Y.L. Bai, Damage evaluation and damage localization of rock, Theoretical and Applied Fracture Mechanics 42 (2) (2004) 131–138.
[10] Y.S. Pan, X.B. Wang, Z.V. Li, Analysis of the strain softening size effect for rock specimens based on shear strain gradient plasticity theory, International Journal of Rock Mechanics and Mining Science 39 (6) (2002) 801–805.
[11] D.A. Lockner, et al., Quasi-static fault growth and shear fracture energy in granite, Nature 350 (6313) (1991) 39–42.
[12] S.C. Yuan, J.P. Harrison, A review of the state of the art in modeling progressive mechanical breakdown and associated fluid flow in intact heterogeneous rocks, International Journal of Rock Mechanics and Mining Science 43 (7) (2006) 1001–1022.